Human Molecular Genetics, 2015, Vol. 24, No. 9 2552–2564

doi: 10.1093/hmg/ddv019
Advance Access Publication Date: 23 January 2015
Original Article

ORIGINAL ARTICLE

FGFR1 signaling in hypertrophic chondrocytes is attenuated by the Ras-GAP neurofibromin during endochondral bone formation

Matthew R. Karolak[1,2], Xiangli Yang[1,2,3] and Florent Elefteriou[1,2,3,4,*]

[1]Department of Pharmacology , [2]Vanderbilt Center for Bone Biology , [3]Department of Medicine and [4]Department of Cancer Biology, Vanderbilt University Medical Center, Nashville, TN 37232, USA

*To whom correspondence should be addressed at: Vanderbilt Center for Bone Biology, Department of Medicine, Vanderbilt University, 2215 Garland Avenue, Light Hall 1255, Nashville, TN 37232, USA. Tel: +1 6153227975; Fax: +1 6153432611; Email: florent.elefteriou@vanderbilt.edu

Abstract

Aberrant fibroblast growth factor receptor 3 (FGFR3) signaling disrupts chondrocyte proliferation and growth plate size and architecture, leading to various chondrodysplasias or bone overgrowth. These observations suggest that the duration, intensity and cellular context of FGFR signaling during growth plate chondrocyte maturation require tight, regulated control for proper bone elongation. However, the machinery fine-tuning FGFR signaling in chondrocytes is incompletely defined. We report here that neurofibromin, a Ras-GAP encoded by *Nf1*, has an overlapping expression pattern with FGFR1 and FGFR3 in prehypertrophic chondrocytes, and with FGFR1 in hypertrophic chondrocytes during endochondral ossification. Based on previous evidence that neurofibromin inhibits Ras-ERK signaling in chondrocytes and phenotypic analogies between mice with constitutive FGFR1 activation and *Nf1* deficiency in *Col2a1*-positive chondrocytes, we asked whether neurofibromin is required to control FGFR1-Ras-ERK signaling in maturing chondrocytes *in vivo*. Genetic *Nf1* ablation in *Fgfr1*-deficient chondrocytes reactivated Ras-ERK1/2 signaling in hypertrophic chondrocytes and reversed the expansion of the hypertrophic zone observed in mice lacking *Fgfr1* in *Col2a1*-positive chondrocytes. Histomorphometric and gene expression analyses suggested that neurofibromin, by inhibiting *Rankl* expression, attenuates pro-osteoclastogenic FGFR1 signaling in hypertrophic chondrocytes. We also provide evidence suggesting that neurofibromin in prehypertrophic chondrocytes, downstream of FGFRs and via an indirect mechanism, is required for normal extension and organization of proliferative columns. Collectively, this study indicates that FGFR signaling provides an important input into the Ras-Raf-MEK-ERK1/2 signaling axis in chondrocytes, and that this input is differentially regulated during chondrocyte maturation by a complex intracellular machinery, of which neurofibromin is a critical component.

Introduction

Endochondral bone formation is a complex, highly regulated and orderly multi-step process by which long bones elongate during development and heal following fracture. It relies on tight spatio-temporal interactions and crosstalk between growth factors and signaling from their receptors in target cells, including osteo-chondroprogenitors, chondrocytes, osteoblasts and osteoclasts. Proper signaling within the growth plate between chondrocytes and with neighboring cells is essential for the successful and timely transition of resting chondrocytes to proliferating and then hypertrophic chondrocytes (1,2). Failure or dysregulation of any of these steps during development typically leads to shortened stature or dwarfism, structural bone abnormalities (3), whereas failure during fracture healing in adults leads to fracture non-union (pseudarthrosis) (4).

Fibroblast growth factor (FGF) signaling during endochondral bone formation has been the subject of intense scientific inquiry. In the growth plate, the receptors for FGFs (mainly FGFR3 and FGFR1) were shown to be expressed in distinct zones: FGFR3 in

Received: November 11, 2014. **Revised:** December 30, 2014. **Accepted:** January 20, 2015

proliferating chondrocyte columns and FGFR1 in hypertrophic chondrocytes (5–9). Constitutive FGFR3 activity in the growth plate, caused by activating *Fgfr3* mutations, inhibits chondrocyte proliferation, leading to growth arrest and inhibition of maturation to hypertrophy (10–12). Molecularly, activating *FGFR3* mutations cause overactive downstream ERK and STAT1 signaling in the developing growth plate, leading to several forms of dwarfism which vary in severity depending on the degree of FGFR3 constitutive activity and ERK activity (13–19). The function of FGFR1 in endochondral bone growth, on the other hand, remains unclear. Activating *FGFR1* mutations have been associated with craniosynostoses, caused by defects in intramembranous ossification (20–22). In the growth plate, the non-overlapping expression patterns of FGFR1-FGFR3 suggest that these receptors have unique functions, mediated by differences in their ligand-binding specificity and/or downstream signaling. In addition, human cases indicate that FGFR1 signaling is crucially important for endochondral ossification. Activating mutations in *FGFR1* indeed cause osteoglophonic dysplasia, a rare syndrome characterized by rhizomelic dwarfism, craniosynostosis and non-ossifying bone lesions, fracture healing deficits, scoliosis, tibial bowing, low bone mineral density, hypertelorism and pectus excavatum (23–28).

Activation of ERK1/2 and p38 in response to FGF has been observed in multiple cell types, whereas the activities of the JNK kinases, the PI3K-AKT pathway and the PLCγ pathway vary depending on cell type (29). FGF treatment of RCS chondrocytes and PC12 adrenal cells, which leads to growth arrest, was shown to be accompanied by strong and sustained ERK1/2 activation, whereas epidermal growth factor (EGF) treatment, was not (30,31). These results suggest the existence of cell-specific and possibly differentiation stage-specific mechanisms to control the intensity or duration of FGFR-Grb2-Sos-Ras-Raf-MEK-ERK signaling.

One of the intracellular regulators of this pathway is neurofibromin, a Ras GTPase activating protein (Ras-GAP) that promotes the conversion of active Ras bound to GTP to the inactive form of Ras bound to GDP. Loss-of-function mutations in *NF1*, the gene encoding neurofibromin, causes chronic and unregulated Ras and ERK1/2 activity, which is at the origin of the multiple conditions associated with neurofibromatosis type-1 (NF1). Approximately 40% of individuals with NF1 display skeletal pathologies, including non-ossifying bone lesions, pseudarthrosis, shortened stature, idiopathic or dystrophic scoliosis, asymmetry of facial bones, osteosclerosis, tibial bowing, hypertelorism, pectus excavatum and low bone mineral density (32–36), which are reminiscent of the bone manifestations observed in individuals with osteoglophonic dysplasia, although more focal and heterogeneous than the latter. Our previous studies have shown that *Nf1* deletion in *Col2a1*-positive murine chondrocytes leads to Ras-ERK1/2 chronic activation, to a reduction in the proliferation and hypertrophic zones of the growth plate and to dwarfism compared with wild-type (WT) littermates (37,38). In addition, these mice display increased number of osteoclasts at the osteochondral border, and *Nf1*-deficient chondrocytes favored osteoclastogenesis *ex vivo*, suggesting that in chondrocytes, neurofibromin serves to limit osteoclastogenesis and growth plate catabolism during development.

Genetic mouse models with *Nf1* deficiency or *Fgfr1* gain- or loss-of-function mutations support a negative association between FGFR1 signaling and neurofibromin activity. First, we found that the activation of ERK1/2 by FGF2 treatment is dampened to baseline activity within 30 min in WT chondrocytes, whereas it lasts more than 1 h in *Nf1*-deficient chondrocytes. These findings suggested that neurofibromin acts as a brake on FGFR signaling in chondrocytes (38). Second, the hypertrophic zone of $Fgfr1^{Col2cKO}$ mice, in which *Fgfr1* is ablated in *Col2a1*-positive chondrocytes, is longer than in WT littermates, in contrast to the shortened hypertrophic zones of the $Nf1^{Col2cKO}$ mice, which lack *Nf1* in the same *Col2a1*-positive cells (7,38). Third, $Fgfr1^{Pro250Arg}$ mice, harboring a constitutively active $Fgfr1^{Pro250Arg}$ allele at the endogenous *Fgfr1* locus (39), are dwarfed as are $Nf1^{Col2cKO}$ mice (37–39). Lastly, at the molecular level, the growth plate expression of matrix metalloproteinase 9 (*Mmp9*) and osteopontin (*Opn*), two proteins contributing to growth plate catabolism and osteoclastogenesis at the osteochondral front, are downregulated in $Fgfr1^{Col2cKO}$ mice while they are upregulated in $Nf1^{Col2cKO}$ mice (7,38). Therefore, constitutive activation of FGFR1 in $Fgfr1^{Pro250Arg}$ mice leads to similar phenotypes to the ones observed in $Nf1^{Col2cKO}$ mice lacking *Nf1* in chondrocytes, whereas loss of FGFR1 in $Fgfr1^{Col2cKO}$ mice triggers phenotypes that are mostly opposite to the ones observed in $Nf1^{Col2cKO}$ mice. Collectively, these observations led us to hypothesize that neurofibromin acts as a brake on FGFR1 signaling in the developing growth plate. In this study, we generated double mutant mice lacking both *Nf1* and *Fgfr1* in *Col2a1*-positive chondrocytes to ask whether loss of activity of neurofibromin and thus activation of Ras-ERK1/2 signaling reverses the aberrant hypertrophic zone length and decreased osteoclastogenesis caused by lack of FGFR1 signaling in $Fgfr1^{Col2cKO}$ mice (Fig. 1B). Our results support a model whereby neurofibromin controls: (i) the cartilage catabolism-promoting function of FGFR1 signaling in hypertrophic chondrocytes and (ii) the organization and extension of proliferative chondrocyte columns, via regulation of FGFR3 (and possibly FGFR1) signaling in prehypertrophic chondrocytes.

Results

Fgfr1, *Fgfr3* and *Nf1* expression is localized to distinct zones in the growth plate

A first requirement for neurofibromin to control FGFR1 signaling is for the two proteins to be expressed in the same chondrocyte population. To address this question, we performed *in situ* hybridization (ISH) on serial paraffin sections on postnatal (P) WT long bone growth plates, using Indian hedgehog (*Ihh*) as a marker of the prehypertrophic zone. At both P0 and P7, *Fgfr1* and *Nf1* transcripts were both detected in the hypertrophic zone, with minimal detectable expression in the proliferation zone, where *Fgfr3* was localized primarily. Both *Fgfr1* and *Nf1* transcripts had weaker expression detectable in the prehypertrophic zone (Fig. 1A). Thus *Fgfr1* expression overlapped with *Nf1* expression in the prehypertrophic, hypertrophic and perichondrium areas, while *Fgfr3* expression only overlapped with *Nf1* expression in prehypertrophic chondrocytes at both P0 and P7. Although co-expression does not prove functional interaction, these results suggest that neurofibromin may regulate FGFR1 signaling rather than FGFR3 signaling in hypertrophic growth plate chondrocytes.

Nf1 ablation in *Fgfr1*-deficient chondrocytes reverses the alterations in growth plate maturation/hypertrophy observed in $Fgfr1^{Col2cKO}$ mice

The overlap in *Fgfr1* and *Nf1* expression in postmitotic prehypertrophic and hypertrophic chondrocytes (Fig. 1A and (5,7,9,38,40)), the largely opposite growth plate phenotypes between $Fgfr1^{Col2cKO}$ and $Nf1^{Col2cKO}$ mice (7,37,38) and the fact that FGFR activation and *Nf1* mutation/ablation both trigger Ras-Raf-MEK-ERK activation

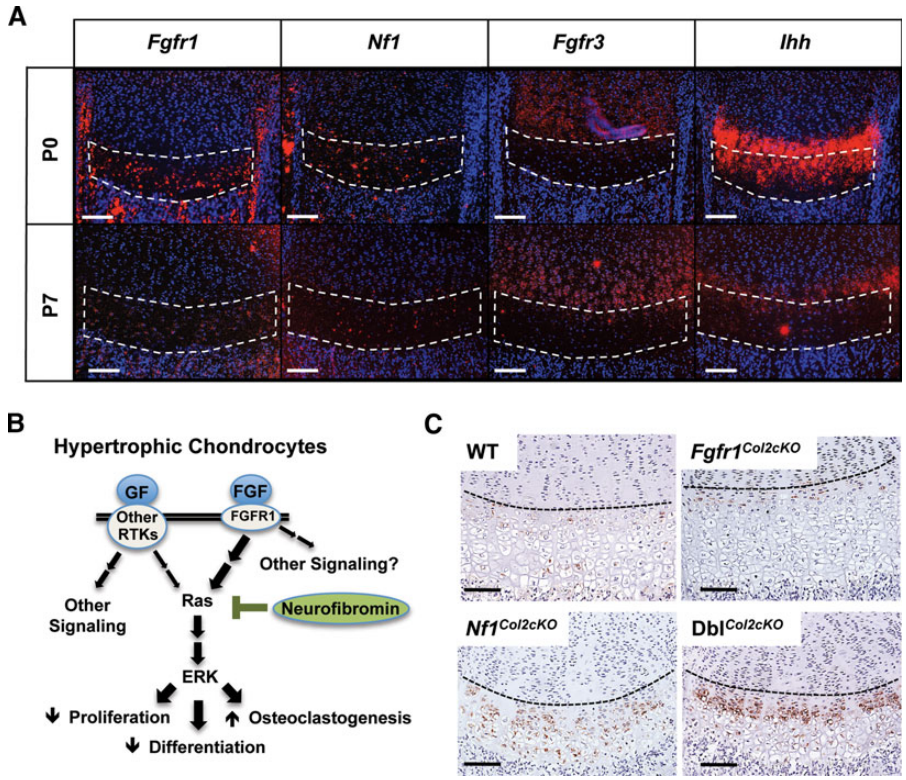

Figure 1. *Fgfr1*, *Fgfr3* and *Nf1* expression is localized to distinct zones in the growth plate. (**A**) *Fgfr1*, *Fgfr3* and *Nf1* localize to distinct zones of the growth plate across early postnatal development. *In situ* hybridization (red signal) on serial distal femur sections shows that *Fgfr1* localizes to prehypertrophic and hypertrophic chondrocytes at P0 (top row) and P7 (bottom row). *Nf1* is expressed in prehypertrophic and hypertrophic chondrocytes at P0 and P7. *Fgfr3* localizes in the proliferation and prehypertrophic zones at P0 and P7. *Ihh* marks the prehypertrophic zone. Hoechst stained nuclei appear in blue. White boxes denote hypertrophic zones. Scale bar: 100 μm. (**B**) Schematic of FGFR1 signaling in hypertrophic chondrocytes. We hypothesized that FGFR1 is a major Ras/ERK activator in hypertrophic chondrocytes that is tempered by the Ras-GAP activity of neurofibromin. (**C**) Immunohistochemistry for phospho-ERK in P7 WT, $Fgfr1^{Col2cKO}$, $Nf1^{Col2cKO}$ and $Dbl^{Col2cKO}$ proximal tibial growth plates shows basal staining in WT, reduced activation in $Fgfr1^{Col2cKO}$ and elevated activation in $Nf1^{Col2cKO}$ and $Dbl^{Col2cKO}$ hypertrophic chondrocytes. Brown signal indicates phospho-ERK; sections are counterstained with hematoxylin. Black lines delineate proliferation and prehypertrophic zones. Scale bar: 100 μm.

in chondrocytes (38), led us to the hypothesis that neurofibromin inhibits, among the many receptor tyrosine kinases (RTKs) expressed in the growth plate, the signaling of FGFR1 in mature chondrocytes (Fig. 1B). This hypothesis is not functionally testable *in vitro* due to the dynamic nature of growth plate development and challenges in generating maturing chondrocytes *in vitro*, and can be best addressed genetically and *in vivo*, by either overexpressing neurofibromin in chondrocytes to rescue the phenotypes of cells with activation of FGFR1, or by reducing neurofibromin activity in cells lacking FGFR1 to artificially reactivate Ras-ERK1/2 signaling in these cells. In the latter option, we reasoned that lack of neurofibromin, leading to Ras-ERK1/2 pathway activation (38) (Fig. 1C, bottom left and right), in *Fgfr1*-deficient chondrocytes (in which Ras-ERK1/2 signaling is reduced, Fig. 1C, top right), should reverse the growth plate phenotypes of $Fgfr1^{Col2cKO}$ mice. We thus generated double mutant mice lacking both *Nf1* and *Fgfr1* in *Col2a1*-expressing chondrocytes ($Dbl^{Col2cKO}$ mice) and compared their skeletal phenotypes to single knockout, $Fgfr1^{Col2cKO}$ and $Nf1^{Col2cKO}$ littermates.

Gross examination over the period of rapid growth before weaning indicated that both body length (Fig. 2A) and body weight (Supplementary Material, Fig. S1) were reduced in both $Nf1^{Col2cKO}$ and $Dbl^{Col2cKO}$ mice compared with WT littermates and $Fgfr1^{Col2cKO}$ mice. Similarly, both genotypes had significantly shorter bones than WT and $Fgfr1^{Col2cKO}$ mice at P18 (Fig. 2B). $Fgfr1^{Col2cKO}$ mice also had reduced stature (by P4), body weight (by P9) and tibial length (P18) compared with WT littermates, despite the increased size of their hypertrophic zone (Fig. 2D) (7). Body length, body weight and tibia length were not significantly different between $Nf1^{Col2cKO}$ and $Dbl^{Col2cKO}$ mice (Fig. 2A and B).

To assess changes in growth plate structure between WT, single mutant $Fgfr1^{Col2cKO}$ and $Nf1^{Col2cKO}$ and $Dbl^{Col2cKO}$ mice, growth plate histomorphometry was performed, analyzing the FGFR3-rich proliferation and FGFR1-rich hypertrophic zones longitudinally at P0, 7 and 14 days of age. The proliferation zones of all four groups of mice were not significantly different until P14, at which time the proliferation zones of $Nf1^{Col2cKO}$ and $Dbl^{Col2cKO}$ were significantly shorter than that of WT and $Fgfr1^{Col2cKO}$ mice, although they were not statistically different from each other (Fig. 2C). In contrast, the hypertrophic zone across all three postnatal time points was elongated by inactivation of *Fgfr1* in *Col2a1*-expressing chondrocytes (Fig. 2D and E), in agreement with previous studies (7). Ablation of *Nf1* in double mutant $Dbl^{Col2cKO}$ mice reduced the size of this zone compared with WT and $Fgfr1^{Col2cKO}$ littermate mice at P0, 7 and 14, to values similar to the ones observed in $Nf1^{Col2cKO}$ mice (the hypertrophic zones of $Nf1^{Col2cKO}$ and $Dbl^{Col2cKO}$ mice were not statistically different from each other). In addition, lack of *Nf1* in *Fgfr1*-deficient hypertrophic chondrocytes led to disturbances in the orderly stacking of the proliferative chondrocyte columns observed in WT and $Fgfr1^{Col2cKO}$mice (Fig. 2E). Increased phospho-ERK1/2 immunostaining in the growth plate prehypertrophic and hypertrophic regions in $Dbl^{Col2cKO}$ mice compared with $Fgfr1^{Col2cKO}$ mice (Fig. 1C, bottom

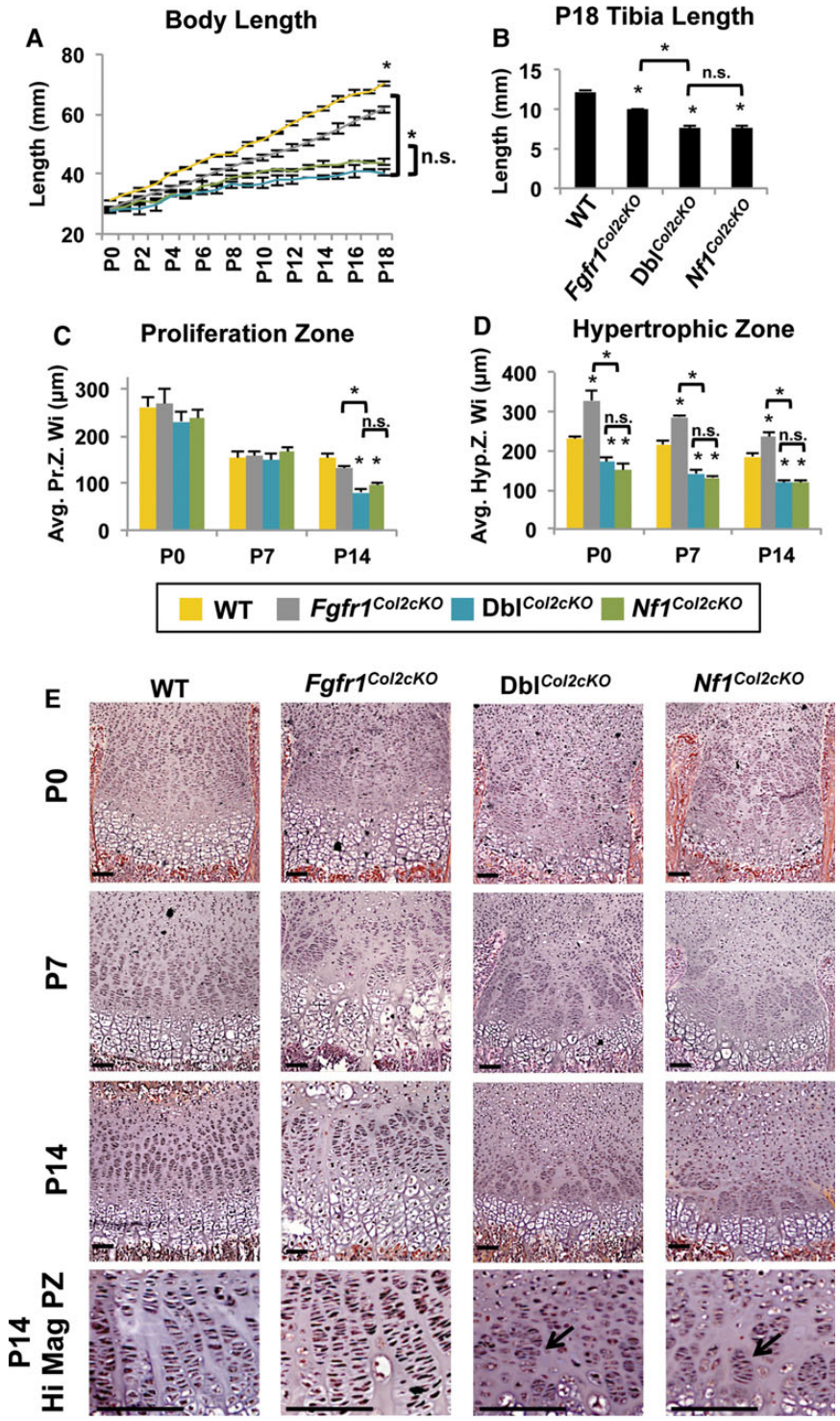

Figure 2. *Nf1* ablation in *Fgfr1*^{Col2cKO} mice reverses their hypertrophic zone phenotype. (**A**) P0–P18 body length of WT, *Fgfr1*^{Col2cKO}, *Nf1*^{Col2cKO} and Dbl^{Col2cKO} mice. Body length was not significantly different between *Nf1*^{Col2cKO} and Dbl^{Col2cKO} mice, but both genotypes had a body length significantly less than WT and *Fgfr1*^{Col2cKO} mice (*$P < 0.05$ versus WT unless indicated, $n = 4$ per group, repeated measure two-way ANOVA). (**B**) P18 tibial length of WT, *Fgfr1*^{Col2cKO}, *Nf1*^{Col2cKO} and Dbl^{Col2cKO} mice. Tibial length was not significantly different between *Nf1*^{Col2cKO} and Dbl^{Col2cKO} mice, but it was significantly less in Dbl^{Col2cKO} than in WT and *Fgfr1*^{Col2cKO} mice (*$P < 0.05$ versus WT unless indicated, $n = 7$ per group, one-way ANOVA). (**C** and **D**) Length quantification of proximal tibial proliferation (C) and hypertrophic (D) zones of P0, 7 and 14 WT, *Fgfr1*^{Col2cKO}, *Nf1*^{Col2cKO} and Dbl^{Col2cKO} mice (*$P < 0.05$ versus WT unless indicated, $n = 4$ per group, two-way ANOVA). The length of the proliferation zones in *Nf1*^{Col2cKO} and Dbl^{Col2cKO} mice were significantly shorter than WT but not significantly different from each other at P14. The same was true of the hypertrophic zone, but at P0, 7 and 14. (**E**) H&E staining of proximal tibial growth plates of WT, *Fgfr1*^{Col2cKO}, *Nf1*^{Col2cKO} and Dbl^{Col2cKO} mice at P0, 7 and 14 and high magnification of the proliferation zone (PZ) at P14. Arrows indicate disorganized proliferative columns. Scale bar: 100 µm.

right) confirmed reactivation of the Ras-ERK1/2 pathway upon *Nf1* ablation in these mice. In addition, *in situ* hybridization and quantitative RT–PCR (qPCR) verified efficient *Fgfr1* deletion in the growth plate of $Fgfr1^{Col2cKO}$ mice and that *Fgfr1* expression was not affected with regard to level of expression or growth plate localization upon *Nf1* ablation (see Fig. 5A and C). Thus, *Nf1* ablation in *Fgfr1*-deficient chondrocytes reverses the increase in growth plate hypertrophic zone observed in $Fgfr1^{Col2cKO}$ mice, and has a deleterious effect on the stacking of the proliferative chondrocyte columns, which was not affected in mice lacking *Fgfr1* only.

Lack of *Nf1* in *Fgfr1*-deficient chondrocytes reverses the reduction in osteochondral osteoclast number observed in $Fgfr1^{Col2cKO}$ mice

Osteoclast number at the chondro-osseous junction (the bone marrow zone immediately adjacent to the growth plate) was shown to be reduced in $Fgfr1^{Col2cKO}$mice, and *Mmp9* and *Opn* expression were lower in *Fgfr1* null chondrocytes compared with WT chondrocytes (7). In contrast, $Nf1^{Col2cKO}$ mice display an increase in osteoclast number at the osteochondral border (37,38,41), and *Nf1* null chondrocytes have elevated expression of *Rankl*, *Opn*, *Mmp9* and *Mmp13*, all of which are important for extracellular bone matrix catabolism (38). These observations suggested that FGFR1 and neurofibromin were both involved, in an antagonistic fashion, in the mechanism by which mature chondrocytes stimulate growth plate catabolism. To determine whether the reduced osteoclast density at the osteochondral border in $Fgfr1^{Col2cKO}$ mice could be rescued by concurrent deletion of *Nf1* in growth plate chondrocytes, we quantified osteoclast number in TRAP-stained thin bone sections from WT, $Nf1^{Col2cKO}$, $Fgfr1^{Col2cKO}$ and $Dbl^{Col2cKO}$ mice. When *Fgfr1* was deleted in *Col2a1*-expressing chondrocytes of newborn and P14 mice, osteoclast number at the chondro-osseous junction was reduced (Fig. 3A–C), in line with previous studies in $Fgfr1^{Col2cKO}$ embryos (7). Upon *Nf1* deletion, a clear increase in the number of TRAP-positive multinucleated osteoclasts was observed in $Dbl^{Col2cKO}$ growth plates versus WT mice. Osteoclast number was not significantly different between $Dbl^{Col2cKO}$ and $Nf1^{Col2cKO}$ growth plates at P0 and P14 (Fig. 3A–C). Consistently, we found that *Rankl* expression was elevated in $Nf1^{Col2cKO}$ and $Dbl^{Col2cKO}$ growth plates, yet decreased in $Fgfr1^{Col2cKO}$ growth plates taken from 5-day-old pups, compared with WT animals (Fig. 3D). *Opg*

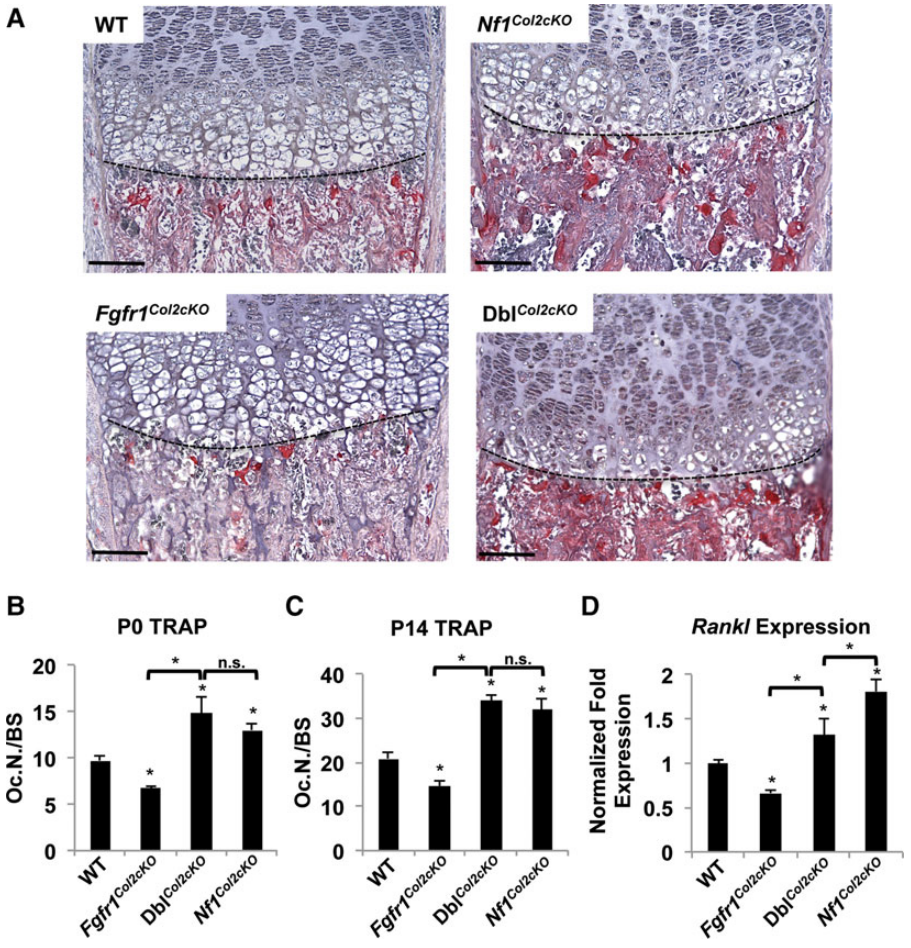

Figure 3. *Nf1* ablation in $Fgfr1^{Col2cKO}$ mice reverses their decrease in osteoclastogenesis at the osteochondral junction. TRAP staining in distal femurs from P0 pups (**A**) and quantification of the number of TRAP-positive (red) osteoclasts per osteochondral border surface (BS) in P0 (**B**) and P14 (**C**) distal femur sections showed that the number of osteoclasts at the chondro-osseous junction in $Fgfr1^{Col2cKO}$ mice is reduced compared with WT littermates, and that *Nf1* deletion in $Dbl^{Col2cKO}$ mice leads to higher number of osteoclasts compared with $Fgfr1^{Col2cKO}$ mice. Osteoclast number in $Nf1^{Col2cKO}$ and $Dbl^{Col2cKO}$ was not significantly different from each other. The osteochondral border surface is indicated by a dotted line (*$P < 0.05$ versus WT unless indicated, $n = 4$ per group, one-way ANOVA, scale bar: 100 μm). (**D**) *Rankl* expression is increased in P5 long bone growth plate cartilage from $Nf1^{Col2cKO}$ and $Dbl^{Col2cKO}$ mice and decreased in $Fgfr1^{Col2cKO}$ P5 growth plate cartilage when compared with WT (*$P < 0.05$ versus WT unless indicated, $n = 4$ per group, one-way ANOVA, qPCR).

expression was unchanged in all four genotypes (Supplementary Material, Fig. S2). These findings suggest that neurofibromin attenuates FGFR1 signaling in hypertrophic growth plate chondrocytes to limit their osteoclastogenic-promoting function.

Nf1 ablation in *Col10a1*-positive hypertrophic chondrocytes reduces hypertrophic zone width but does not impair bone elongation

The results above suggest a predominant role of neurofibromin, downstream of FGFR1, in hypertrophic chondrocytes, however, neurofibromin is also expressed in prehypertrophic chondrocytes (Fig. 1) and osteoblasts (37,38,40). In an effort to determine the function of neurofibromin more specifically in hypertrophic growth plate chondrocytes, we generated $Nf1^{Col10cKO}$ mice lacking *Nf1* in *Col10a1*-positive cells, using the *Col10-Cre* driver transgenic mice (42). We first used these mice bred with *Rosa26:LacZ* reporter mice (43) to examine the activity of the *Col10-Cre* transgene specifically during the active phase of postnatal bone elongation at P0, P7 and P14, since prior studies only reported activity embryonically and shortly after birth (P1, P3) or 5 weeks after birth (42,44,45). We found, at all ages analyzed, that the *Col10-Cre* transgene is active in hypertrophic chondrocytes, as demonstrated by positive β-galactosidase staining in this area of the growth plate, but not in proliferative columns. β-galactosidase activity was also observed in osteoblast-like cells in the primary spongiosa and embedded osteocyte-like cells (Fig. 4A, data not shown). $Nf1^{flox/flox}$ mice were then bred to *Col10-Cre* mice to generate, through two rounds of breeding, $Nf1^{Col10cKO}$ mice and WT littermates. Unexpectedly, $Nf1^{Col10cKO}$ mice had a normal stature and physical appearance at all time points analyzed (from P0 to P18) compared with WT littermates (Fig. 4B). Histologically, the proliferation zone length of $Nf1^{Col10cKO}$ growth plates was not significantly shorter than WT at P0 or P18 (Fig. 4C). The hypertrophic zone of $Nf1^{Col10cKO}$ growth plates was, however, significantly shorter than WT at P0 and P18 (Fig. 4D). We also found that the number of osteoclasts at the chondro-osseous border was significantly higher in $Nf1^{Col10cKO}$ compared with WT mice (Fig. 4E and F). The growth plates of $Nf1^{Col10cKO}$ mice appeared normal with orderly proliferative chondrocyte columns as opposed to the disorganized columns seen in $Nf1^{Col2cKO}$ growth plates, in which *Nf1* is ablated in prehypertrophic and hypertrophic cells (Fig. 4G). Collectively, these results suggests that *Nf1* loss-of-function in prehypertrophic chondrocytes, where *Nf1* expression overlaps with both *Fgfr3* and *Fgfr1*, is responsible for the size and growth plate columnar defects observed in $Nf1^{Col2cKO}$ mice, whereas *Nf1* in hypertrophic chondrocytes primarily regulates osteoclastogenesis in the primary spongiosa.

Fgfr3 expression is not altered upon *Fgfr1* ablation in *Col2a1*-positive chondrocytes

Our analyses suggest that lack of *Nf1* in prehypertrophic chondrocytes causes alterations in the size and organization of *Nf1* and *Fgfr1*-negative, but *Fgfr3*-positive, proliferative chondrocyte columns. Ectopic *Fgfr3* upregulation was previously observed in *Fgfr1*-deficient osteoblasts (7), and it has been shown that chondrocytic FGFR and ERK1/2 signaling in general are inhibitory to chondrocyte proliferation/differentiation (although these effects were not attributed to an individual or specific FGF receptor) (11,46). These observations prompted us to question whether *Nf1* or *Fgfr1* deficiency altered growth plate *Fgfr3* expression level or tissue localization, thus potentially causing some of the observed changes in proliferation and hypertrophic zones. Hence, we assessed *Fgfr3* expression by *in situ* hybridization and qPCR analyses in the growth plates of $Nf1^{Col2cKO}$ and $Dbl^{Col2cKO}$ mice. We found that *Fgfr3* expression was not mislocalized when *Nf1* was deleted alone or in combination with *Fgfr1*, and remained primarily in the proliferation zone of the growth plate with some expression in the prehypertrophic zone at P0 (Fig. 5A). Furthermore, quantitative assessment by qPCR showed no significant differences in *Fgfr3* expression in $Fgfr1^{Col2cKO}$, $Nf1^{Col2cKO}$ and $Dbl^{Col2cKO}$ growth plates versus WT growth plates 5 days after birth (Fig. 5B and C).

We also sought to confirm whether expression levels and localization of *Fgfr1* were altered by *Nf1* deletion in $Nf1^{Col2cKO}$ growth plates, and the efficiency of *Fgfr1* deletion with the *Col2-Cre* driver. We found that *Fgfr1* was normally localized in $Nf1^{Col2cKO}$ growth plates and that *Fgfr1* expression was, as expected, reduced in $Dbl^{Col2cKO}$ growth plates (Fig. 5A, left column). Quantitatively, *Fgfr1* expression was efficiently lowered using the *Col2*-Cre driver as assessed by qPCR on P5 growth plates and was not reduced in $Nf1^{Col2cKO}$ growth plates (Fig. 5C). Together, these results confirm efficient *Fgfr1* recombination in $Fgfr1^{Col2cKO}$ and $Dbl^{Col2cKO}$ mutant mice, and indicate that *Fgfr3* expression is not upregulated in response to *Fgfr1* ablation in these two models.

Pan-FGFR inhibition with BGJ-398 enhances bone growth in $Nf1^{Col2cKO}$ mice

The difference in bone size between $Nf1^{Col2cKO}$ and $Nf1^{Col10cKO}$ mice and the overlap of expression between *Nf1*, *Fgfr1* and *Fgfr3* in the prehypertrophic zone suggested that neurofibromin in prehypertrophic chondrocytes may control either FGFR3 or FGFR1 signaling and the mechanism by which these cells inhibit chondrocyte proliferation and column stacking. To address this question and because of the difficulties in generating triple conditional knockout mice lacking *Fgfr1*, *Fgfr3* and *Nf1* with proper littermate controls, we chose to administer the pan-FGFR inhibitor BGJ-398 (47) or vehicle subcutaneously and daily to WT and $Nf1^{Col2cKO}$ newborns. We assessed body weight, body length, tibial length and growth plate parameters at the termination of the experiment 18 days later. Pan-FGFR inhibition by this dose of BGJ-398 reduced ERK1/2 activation in both prehypertrophic and hypertrophic chondrocytes in $Nf1^{Col2cKO}$ mice when compared with vehicle-treated animals (Supplementary Material, Fig. S3A), confirming that the drug was active and acting, at least in part, directly on growth plate chondrocytes. BGJ-398 significantly improved tibial length and the lengths of the proliferation and hypertrophic zones in the growth plates of $Nf1^{Col2cKO}$ mice (Fig. 6A–C), whereas it did not impact bone growth in WT mice. Body length and weight in $Nf1^{Col2cKO}$ mice treated by BGJ-398 were improved compared with vehicle control, but the differences did not reach statistical significance for these two parameters (Fig. 6D and Supplementary Material, Fig. S3B). Noticeably, BGJ-398 treatment improved the columnar organization of the proliferation zone (Fig. 6E). Since the proliferation zone in $Fgfr1^{Col2cKO}$ mice is normal in terms of width and organization, and since *Nf1* is not detectable in this zone, this effect of pan-FGFR inhibition on the width and organization of the proliferation zone in $Nf1^{Col2cKO}$ mice suggests that neurofibromin in prehypertrophic chondrocytes, and downstream of FGFR3 mainly, is required for normal chondrocyte proliferation and column stacking.

Discussion

The respective role of FGFs and FGFRs in the growth plate, the intracellular machinery mediating their activity, and in

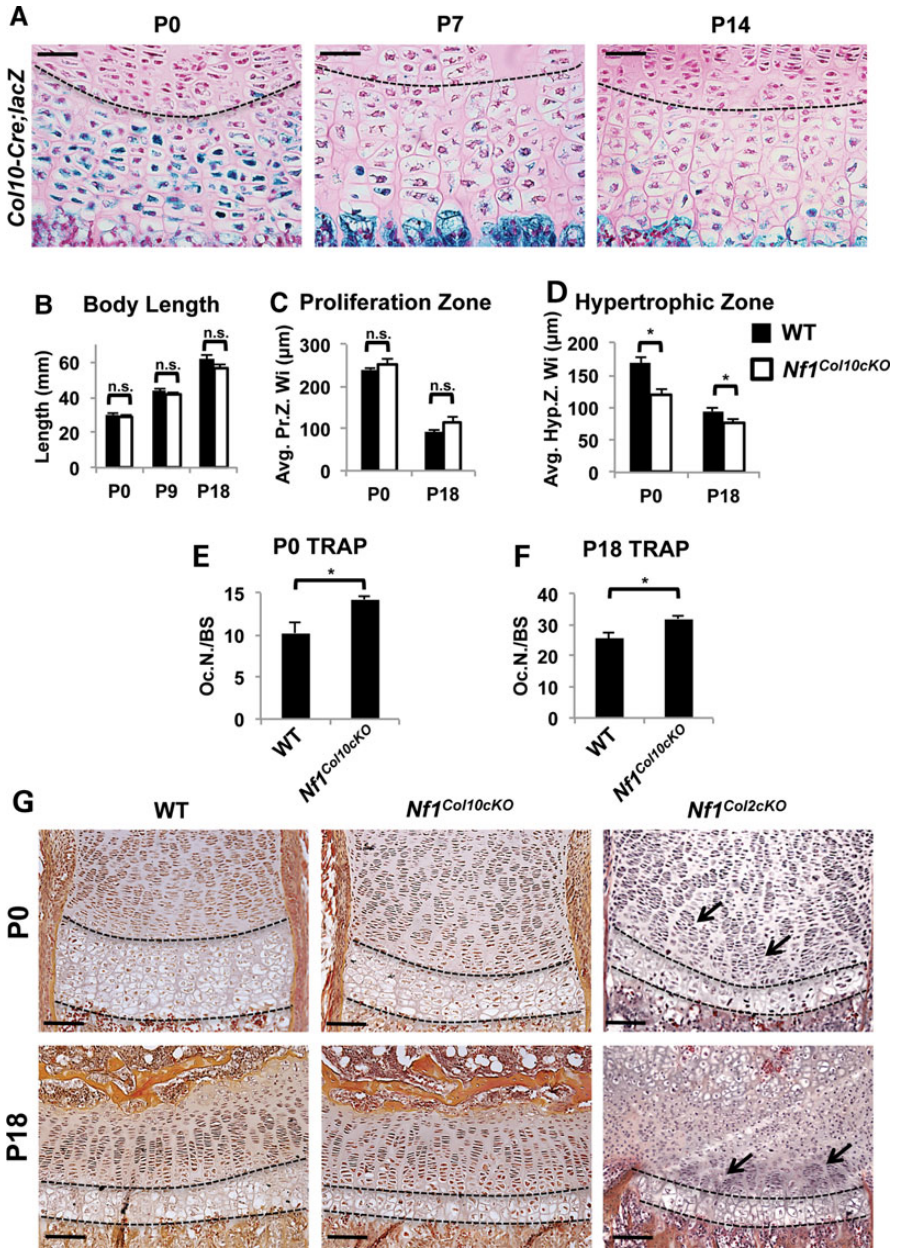

Figure 4. *Nf1* ablation in hypertrophic chondrocytes does not affect bone size but increases osteochondral osteoclastogenesis. (**A**) β-galactosidase staining (blue) in P0, 7 and 14 proximal, *Col10-Cre;Rosa26:lacZ* tibiae shows *Col10-Cre* transgene activity in hypertrophic chondrocytes and primary spongiosa osteoblasts, but not in prehypertrophic chondrocytes. Sections were counterstained with nuclear fast red. Black dotted lines delineate prehypertrophic and hypertrophic zones. Scale bar: 50 μm. (**B**) The body length of $Nf1^{Col10cKO}$ versus WT mice is not significantly different at P0, 9 or 18 (*:$P < 0.05$ versus WT, $n = 5$ per group, repeated measure two-way ANOVA). (**C** and **D**) Length quantification of proximal tibial proliferation (C) and hypertrophic (D) zones of P0 and 18 WT and $Nf1^{Col10cKO}$ mice (*$P < 0.05$ versus WT, $n = 5$ per group, unpaired *t*-test). The length of the proliferation and hypertrophic zones between WT and $Nf1^{Col10cKO}$ mice were not significantly different at P0 or P18. (**E** and **F**) TRAP quantification of the number of TRAP-positive (red) osteoclasts per osteochondral border surface in P0 (E) and P18 (F) proximal tibial sections showed that the number of osteoclasts at the chondro-osseous junction in $Nf1^{Col10cKO}$ mice was significantly greater than WT (*$P < 0.05$ versus WT, $n = 5$ per group, unpaired *t*-test, scale bar: 100 μm). (**G**) H&E staining of proximal tibial growth plates of WT (left column) and $Nf1^{Col10cKO}$ (middle column) littermates at P0 and P18. $Nf1^{Col2cKO}$ proximal tibial growth plates (right column) are shown for comparison, with arrows highlighting disorganized proliferative columns and black dotted lines delineating the hypertrophic zones. Scale bar: 100 μm.

particular the potential contribution of Ras-GAP proteins to these activities remain incompletely characterized, in part because of the dynamic and complex nature of the process of endochondral bone formation and the overlap in expression and signaling pathways downstream of FGFRs. This study provides the first comprehensive experimental and genetic evidence indicating that the Ras-GAP activity of neurofibromin is required in prehypertrophic chondrocytes for normal growth plate elongation and proliferative column organization, and is required in hypertrophic chondrocytes, downstream of FGFR1, to attenuate the osteoclastogenic properties of these cells in contact with the bone marrow environment, and thus the coupling between chondrogenesis and bone modeling during development.

A number of signaling proteins are phosphorylated in response to chondrocyte FGF stimulation, including Shc, PLCγ, STAT1, Gab1 and FRS2α (48–50). These signaling events lead to

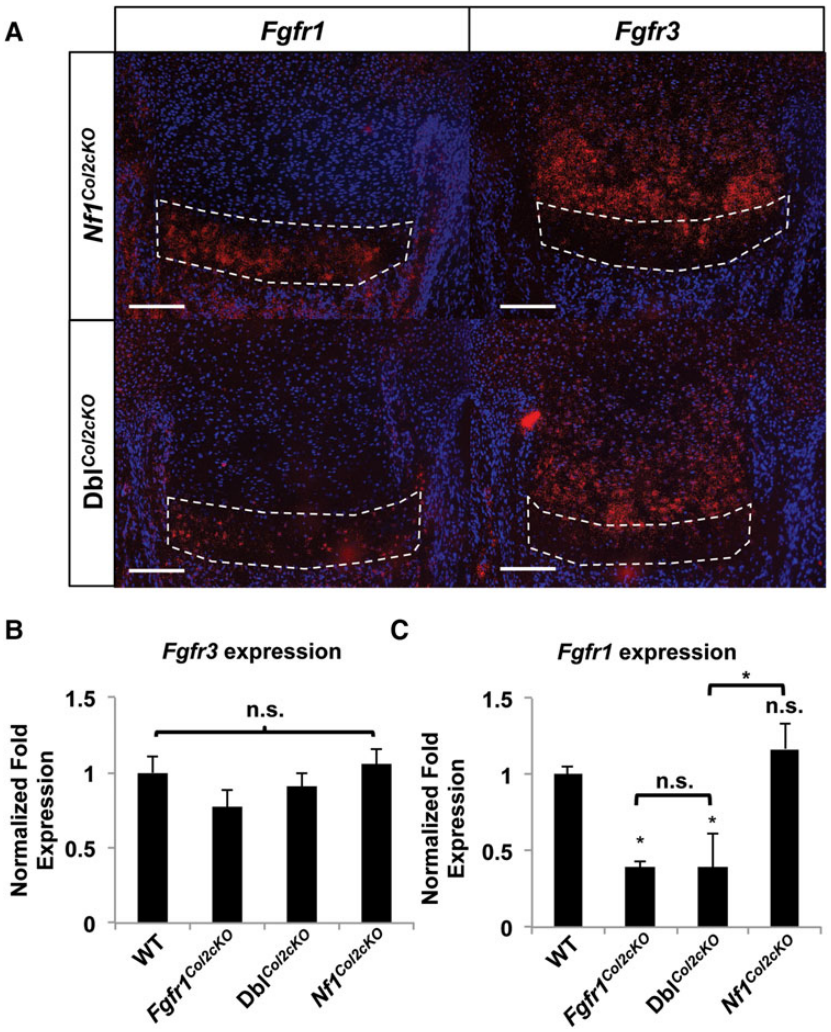

Figure 5. *Fgfr3* expression is not altered upon *Fgfr1* ablation in *Col2a1*-positive chondrocytes. (**A**) *In situ* hybridization (red signal) in P0 distal femora shows that *Fgfr1* expression (left column) remains localized to hypertrophic chondrocytes in *Nf1* null chondrocytes and has a less intense signal in $Dbl^{Col2cKO}$ growth plates (bottom left). *Fgfr3* expression (right column) remains restricted to the proliferation and prehypertrophic zones in $Nf1^{Col2cKO}$ (upper right) and $Dbl^{Col2cKO}$ (lower right) growth plates. Hoechst stained nuclei appear in blue. White boxes denote hypertrophic zones. Scale bar: 100 μm. (**B**) *Fgfr3* expression is not significantly different in P5 long bone growth plate cartilage between WT, $Fgfr1^{Col2cKO}$, $Dbl^{Col2cKO}$ and $Nf1^{Col2cKO}$ mice (one-way ANOVA, $n = 4$ per group, qPCR). (**C**) *Fgfr1* expression is reduced in P5 long bone growth plate cartilage from $Fgfr1^{Col2cKO}$ and $Dbl^{Col2cKO}$ mice when compared with WT, while there is no significant difference in *Fgfr1* expression between $Nf1^{Col2cKO}$ and WT mice (*$P < 0.05$ versus WT unless indicated, $n = 4$ per group, one-way ANOVA, qPCR).

the activation of intracellular signaling pathways that control cell shape, proliferation, differentiation, migration and survival. In particular, the docking proteins FRS2α and FRS2β are major mediators of the Ras/MAPK and PI3K/AKT signaling pathways that fine-tune the signal initiated by FGFR stimulation by negative feedback mechanisms. This study identifies the Ras-GAP neurofibromin as one critical intracellular components controlling FGFR signaling, specifically in postmitotic growth plate chondrocytes, and further supports the notion that the intensity or duration of FGFR signals during endochondral bone formation must be tightly controlled for harmonious development of the growth plate.

Dwarfism in humans is primarily attributed to FGFR3-activating mutations and the resulting lack of extension of the growth plate proliferating zone (13–16), where FGFR3 is highly expressed. FGFR3 activation affects chondrocyte proliferation in a cell-autonomous fashion but also indirectly via repression of IHH signaling (51). Global knockout of *Fgfr3* on the other hand produces mice with a bone overgrowth phenotype including expanded proliferation and hypertrophic zones, enhanced osteoblast differentiation and enhanced osteoclastogenesis (9,52). In contrast to $Fgfr3^{-/-}$ mice, chondrocyte proliferation is reduced in $Nf1^{Col2cKO}$ mice (38), but the width of the proliferation zone is not affected in $Nf1^{Col10cKO}$ mice. Because *Nf1* is expressed in prehypertrophic and hypertrophic chondrocytes, but not detectable in proliferating chondrocytes, these results suggest that neurofibromin is required in prehypertrophic chondrocytes to indirectly control the extension and organization of proliferative chondrocyte columns. This conclusion is further supported by the beneficial effect of pan-FGFR inhibition on bone size, proliferation zone width and columnar organization in growing $Nf1^{Col2cKO}$ mice (although other systemic or indirect effects of the drug cannot be excluded). These results, along with the fact that $Fgfr1^{Col2cKO}$ mice have no proliferation zone size phenotype and that *Fgfr1*-null prehypertrophic chondrocytes still are positive for phospho-ERK (Fig. 1C), suggest that in prehypertrophic chondrocytes, neurofibromin controls FGFR3 signaling to regulate, in an indirect, paracrine fashion, chondrocyte proliferation zone

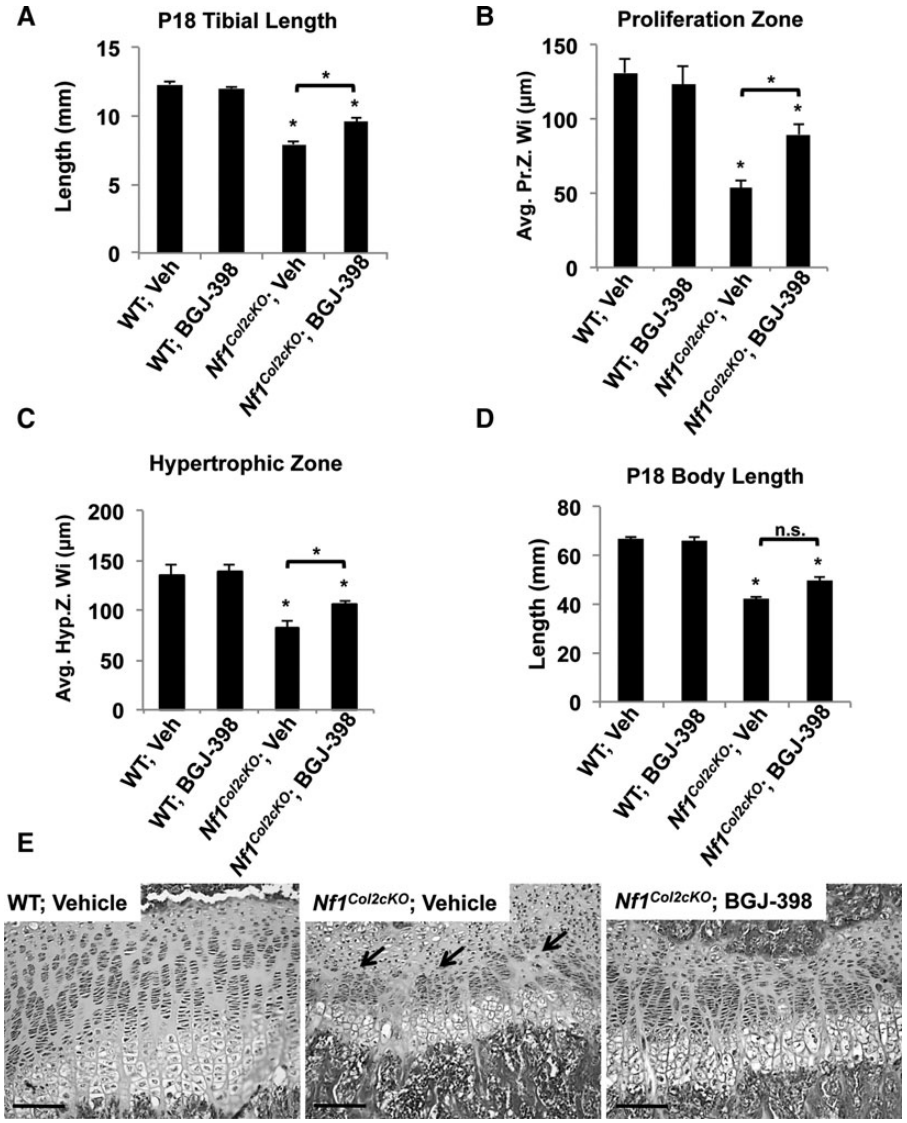

Figure 6. FGFR inhibition with BGJ-398 enhances bone growth in $Nf1^{Col2cKO}$ mice. (**A**) P18 tibial length of $Nf1^{Col2cKO}$ mice treated daily with 10 mg/kg BGJ-398 for 18 days after birth were improved compared with $Nf1^{Col2cKO}$ mice treated with vehicle, while there was no difference between WT animals treated with vehicle or BGJ-398 (*$P < 0.05$ versus WT, vehicle unless indicated, $n = 6$ per group, one-way ANOVA). (**B** and **C**) Length quantification of proliferation (B) and hypertrophic (C) zone lengths at P18 in WT and $Nf1^{Col2cKO}$ littermates treated daily with BGJ-398 or vehicle. BGJ-398 treatment significantly improved both proliferation and hypertrophic zone width in $Nf1^{Col2cKO}$ mice but not in WT mice (*$P < 0.05$ versus WT, vehicle unless indicated, $n = 6$ per group, one-way ANOVA). (**D**) P18 body length of $Nf1^{Col2cKO}$ mice treated with BGJ-398 for 18 days after birth trended towards improvement compared with $Nf1^{Col2cKO}$ mice treated with vehicle, while there was no difference between WT animals treated with vehicle or BGJ-398. (*$P < 0.05$ versus WT, vehicle unless indicated, $n = 6$ per group, one-way ANOVA). (**E**) H&E staining of P18 distal femora growth plates of WT, vehicle-treated (left), $Nf1^{Col2cKO}$, vehicle-treated (middle) and $Nf1^{Col2cKO}$, BGJ-398-treated (right) littermates showing improved columnar structure and zone lengths in $Nf1^{Col2cKO}$, BGJ-398-treated mice versus $Nf1^{Col2cKO}$ vehicle-treated growth plates. Arrows indicate disorganized proliferative columns. Scale bar: 100 µm.

length and their typical columnar organization. This does not rule out a role of FGFR1 signaling in prehypertrophic chondrocytes, based on the severe dwarfism of individuals with osteoglophonic dysplasia and mice with *FGFR1*-activating mutations.

Concurrent ablation of *Nf1* and *Fgfr1* in the same *Col2a1*-expressing cell population and at the same time during development reversed the increase in hypertrophic zone width observed in $Fgfr1^{Col2cKO}$mice. These findings suggest that reactivation of the Ras-Raf-MEK-ERK1/2 pathway by *Nf1* deletion in *Fgfr1*-deficient hypertrophic chondrocytes functionally compensated for the reduced FGFR1 signaling in these cells *in vivo*. We have shown in a previous study that neurofibromin controls *Rankl* expression and osteoclastogenesis in mature chondrocytes, and thus that increased growth plate catabolism likely contributes to the reduction in hypertrophic width observed in $Nf1^{Col2cKO}$ mice (38). The observation that chondrocytic ablation of *Nf1* reverses the reduction in osteoclast number observed in $Fgfr1^{Col2cKO}$ mice, and the fact that the hypertrophic zone width in $Nf1^{Col10cKO}$ mice is shorter (while being longer in $Fgfr1^{Col2cKO}$ mice) compared with WT mice, suggests that neurofibromin, in hypertrophic chondrocytes, inhibits the pro-osteoclastogenic signals from FGFR1 in the chondrocytic lineage. It remains to be determined if activation of the transcription factor ATF4, resulting from the lack of *Nf1*, contributes to the observed increase in *Rankl* expression, as was previously shown in mature osteoblasts (53). Though RANKL and OPG are obvious candidates to mediate changes in osteoclastogenesis at the osteochondral border, and though we indeed observed significant changes in *Rankl* expression *in vivo*,

we cannot rule out the possibility that other pro- or anti-osteoclastogenic molecules are differentially regulated in the presence/absence of neurofibromin or FGFR1. It must also be emphasized that the relatively modest increase in *Rankl* expression in the growth plates of $Nf1^{Col2cKO}$ mice is to be expected based on the nature of the cells expressing this cytokine in the growth plate, i.e. hypertrophic chondrocytes. This area of the growth plate indeed represents a small volume of the growth plate, is under constant catabolism, and contains cells that are hypertrophic (hence less cell number per volume) and rapidly eliminated. These characteristics are even more pronounced in the shortened growth plates of $Nf1^{Col2cKO}$ mice, hence the increase in *Rankl* expression in this transient area cannot be of high amplitude.

The width of the hypertrophic zone depends on multiple factors, including growth plate maturation, catabolism but also chondrocyte apoptosis. However, no difference in chondrocyte apoptosis has been detected between WT mice and mice lacking FGFR1 ($Fgfr1^{Col2cKO}$) (7) or B-Raf (54) or ERK1/2 (55) in *Col2a1*-expressing chondrocytes. On the other hand, we have shown in previous studies that *Nf1*-null chondrocytes have enhanced sensitivity to phosphate-mediated apoptosis *in vitro*, although we failed to detect increased *in vivo* apoptosis in the growth plate of $Nf1^{Col2cKO}$ mice (38). Chondrocyte forced expression of *Spry1*, which leads to ERK activation, as well as an FGFR3-activating mutation, did result in premature chondrocyte apoptosis *in vivo* (56,57), although constitutive activation of MEK1 in these cells did not affect apoptosis (11). Therefore, *Fgfr1* loss-of-function does not alter the rate of chondrocyte apoptosis, but ERK constitutive activation promotes it, via mechanism(s) that remains to be characterized.

Recalcitrant bone healing (pseudarthrosis) affects about 5% of children with NF1. In this condition, tibial bowing is followed by fracture and absence of repair, accumulation of myofibroblasts, non-mineralized matrix and hyaline cartilage, suggesting that the early stages of endochondral bone repair are blocked (58). The developmental phenotypes observed in this study suggest that pan-FGFR inhibition might have a beneficial effect in the setting of NF1 pseudarthrosis on the formation of the cartilaginous callus and its transition to a calcified callus required for bone union following fracture, as bone development recapitulates the main stages of adult bone repair. Although very speculative, this hypothesis can be addressed in preclinical models of NF1 pseudarthrosis, particularly if treatment can be applied locally to avoid undesirable effects on other tissues.

Collectively, our findings thus indicate that neurofibromin in postmitotic growth plate chondrocytes plays an integral part in the Ras-ERK-dependent regulatory mechanisms that allow these cells to integrate and balance signaling from various growth factors via RTKs like FGFRs. These findings are relevant to genetic diseases affecting embryonic development of the skeleton like chondrodysplasias, but also to genetic conditions impacting bone healing in adults, like neurofibromatosis type 1 and RASopathies in general.

Materials and Methods

Animals and drugs

The Vanderbilt University Institutional Animal Care and Use Committee (IACUC) approved all animal procedures. To generate $Dbl^{Col2cKO}$ mice, we employed a two-armed breeding scheme (Supplementary Material, Fig. S4). In arm one, we bred *Col2a1-Cre*;$Fgfr1^{flox/flox}$;$Nf1^{flox/+}$ males with $Fgfr1^{flox/flox}$;$Nf1^{flox/+}$ females to generate WT (cre-negative), $Fgfr1^{Col2cKO}$ (*Col2a1-Cre*;$Fgfr1^{flox/flox}$;$Nf1^{+/+}$;) and $Dbl^{Col2cKO}$(*Col2a1-Cre*;$Fgfr1^{flox/flox}$;$Nf1^{flox/flox}$) mice (59–61). In arm two, we bred *Col2a1-Cre*;$Fgfr1^{flox/+}$;$Nf1^{flox/+}$ males with $Fgfr1^{flox/+}$;$Nf1^{flox/flox}$ females to generate WT (cre-negative), $Nf1^{Col2cKO}$ (*Col2a1-Cre*;$Fgfr1^{+/+}$;$Nf1^{flox/flox}$;) and $Dbl^{Col2cKO}$ (*Col2a1-Cre*; $Fgfr1^{flox/flox}$;$Nf1^{flox/flox}$) mice. Arm two used *Col2a1-Cre*;$Fgfr1^{flox/+}$;$Nf1^{flox/+}$ males rather than *Col2a1-Cre*;$Fgfr1^{flox/+}$;$Nf1^{flox/flox}$ males because *Col2a1-Cre*;$Nf1^{flox/flox}$ mice are infertile. Progenies were obtained at a Mendelian ratio (~12.5% $Fgfr1^{Col2cKO}$, ~6.25% $Nf1^{Col2cKO}$ and ~12.5% or ~6.25% $Dbl^{Col2cKO}$, depending on breeding arm), indicating the absence of embryonic lethality.

$Nf1^{Col10cKO}$ and WT littermate mice were obtained by breeding *Col10-Cre*;$Nf1^{flox/flox}$ males with $Nf1^{flox/flox}$ females (42,60). *Col10-Cre*;*Rosa26:lacZ* mice were obtained by breeding homozygous *Col10-Cre* mice with homozygous ROSA26 reporter mice (43). WT and $Nf1^{Col2cKO}$ littermate mice for drug studies were obtained by breeding *Col2-Cre*;$Nf1^{flox/+}$ males with $Nf1^{flox/flox}$ females (59,60). *Fgfr1* (B6.129S4-*Fgfr1tm5.1Sor/J*) and *Nf1* (STOCK *Nf1tm1Par/J*) floxed mice were obtained from The Jackson Laboratory (Bar Harbor, ME, USA). *Col2-Cre* mice were originally obtained from Dr Gerard Karsenty (Columbia University). *Col10-Cre*;*Rosa26:LacZ* mice were a gracious gift from Dr Douglas Mortlock (Vanderbilt University, Nashville, TN, USA). *Col10-Cre* mice were originally generated by Dr K. von der Mark (University of Erlangen-Nuremberg, Germany).

Tissues were harvested at the indicated times and fixed at 4°C for 24 h in freshly prepared 4% paraformaldehyde (Sigma, St Louis, MO, USA). Body and tibia lengths were assessed by caliper and postmortem Faxitron X-Ray (Tucson, AZ, USA), respectively. Body length was measured while animals were in the prone position and taken from the tip of the nose to the anus with a digital caliper. BGJ-398 (Selleckchem, Houston, TX, USA) or vehicle (PEG300/D5W, 2:1, v/v) was injected subcutaneously daily from birth and for 18 days. BGJ-398 is most potent at FGFRs 1–3 with *in vitro* IC50s of 0.9–1.4 nM but has off target, sub-optimal activity at other non-FGFRs at IC50 concentrations of 180 nM or greater (47).

Histology

Fixed tissues were decalcified for up to 1 week (depending on age) in 20% EDTA at 4°C, followed by dehydration by graded ethanol series, cleared in xylenes (or Histo-Clear for β-galactosidase staining, National Diagnostics, Atlanta, GA, USA) and embedded in paraffin. Serial, 5-micron sagittal sections were cut, Histo-Clear deparaffinized and rehydrated by graded ethanol series. Sections were then stained with hematoxylin and eosin using standard protocols. For osteoclast analyses, sections were TRAP-stained using standard protocols. For β-galactosidase staining, tissues were stained prior to fixation using standard protocols. Briefly, tissues were washed with phosphate buffered 0.02% NP-40, 0.01% deoxycholate and 2 mM $MgCl_2$ followed by overnight incubation in β-galactosidase staining solution (phosphate buffered 0.02% NP-40, 0.01% deoxycholate, 2 mM MgCl2, 5 mM potassium ferricyanide, 5 mM potassium ferrocyanide and 1 mg/ml X-Gal) at room temperature. Tissues were then fixed, decalcified, processed and sectioned as described earlier. Sections were counterstained with nuclear fast red.

Histomorphometric analyses

Histomorphometric measurements were performed using the Bioquant Analysis System (BIOQUANT Image Analysis Corporation, Nashville, TN, USA). To determine the width of the proliferation and hypertrophic zones of the growth plate, we used the

BIOQUANT software to employ a direct measurement technique. Specifically, the border of a zone and the border which constitutes the interface between adjacent zones were identified manually by blinded, properly trained laboratory members. The border between resting chondrocytes and the proliferation zone was defined by the appearance of a proliferative column of four or more chondrocytes of flattened morphology. The interface between the proliferation zone and hypertrophic zones was defined by the appearance of cells of larger size (hypertrophy) at the distal end of proliferative columns. The termination of the hypertrophic zone was defined as the interface between hypertrophic chondrocytes and the primary spongiosa. Along each defined border, BIOQUANT software selected a set of systematically random points with a fixed interval set by the laboratory member. For the neighborhood around each of these points, BIOQUANT computed a vector orthogonal to the interface. Each vector was extended across each respective zone until it intersected the opposite border; the length of each vector was recorded. The width of the zone was then reported as the mean of all such vectors. The width measured by this technique does not attempt to compensate for oblique sectioning, however, all sections included for measurement were orthogonally sectioned and at a similar position within each bone. The osteochondral border surface used for osteoclast measurements was manually defined by blinded, properly trained laboratory members as the interface between the hypertrophic chondrocyte and primary spongiosa compartments, across the entire bone element. Once the interface between these two zones was defined, BIOQUANT computed the length of the interface using standard 2-dimensional distance computations to generate a surface measurement. TRAP-positive osteoclasts in contact with this osteochondral border were counted for analyses.

In situ hybridization (ISH)

Tissues were fixed, decalcified, processed and sectioned as described earlier. Sections were stored at 4°C until use. ISH was performed by standard protocols. *Fgfr1*, *Fgfr3, Ihh* ISH was performed using probes to the respective 3′ UTRs (*Fgfr1* and *Fgfr3* sequences available upon request, *Ihh* as previously published) (62). *Nf1* ISH was performed using a probe to the 5′ translated region of the mRNA (40). Sense and anti-sense [35S]-uridine triphosphate (Perkin Elmer, Waltham, MA, USA) probes were synthesized for hybridization as described previously (62,63). Sections were stained with Hoechst 33258 to identify nuclei. Images were processed using Adobe Photoshop (San Jose, CA, USA).

Immunohistochemistry

Tissues were fixed, decalcified, processed and sectioned as described earlier. Antigens were retrieved on graded ethanol rehydrated sections using DeCal Retrieval Solution per manufacturer's instructions (Biogenex, Fremont, CA, USA). Immunostaining was performed using standard protocols with anti-phospho-p44/42 MAPK (Erk1/2, Thr202/Tyr204, E10 mouse mAb #9106, Cell Signaling, Boston, MA, USA) antibodies or non-immune IgG1 antibodies, followed by ImmPACT NovaRED (Vector Laboratories, Burlingame, CA, USA) horseradish peroxidase detection of the secondary antibody. Immunostained sections were counterstained with hematoxylin.

Genomic PCR, RT–PCR and qPCR

For genotyping, genomic DNA was isolated from tail biopsies by sodium hydroxide digestion and PCR was performed using appropriate primers. The *Nf1* floxed allele was detected with primers P1, P3 and P4, as previously described (60). The *Fgfr1* floxed allele was detected with primers intr5.53 and intr5.53 to generate a 750 bp band for the floxed allele and a 564 bp band for the WT allele, as previously described (61). The *Col2-Cre* transgene was detected using the forward primer: GAGTTGATAGCTGGCT GGTGGCAGATG and reverse: TCCTCCTGCTCCTAGGGCCTCCTG CAT to generate a 700 bp band (59). The *Col10-Cre* transgene was detected using the P1 and P5 primers to generate a 305 bp band, as previously described (42). Total RNA was extracted from snap-frozen P5 (to avoid the presence of the secondary ossification center) murine growth plates (1 distal femoral epiphysis and 1 proximal tibial epiphysis per sample) using TRIzol (Life Technologies, Grand Island, NY, USA), and cDNAs were synthesized from 1 microgram RNAs following DNase I treatment using the high-capacity cDNA reverse-transcription kit (Applied Biosystems, Foster City, CA, USA). Quantitative PCR (qPCR) were performed using TaqMan gene expression assays. The probe and primer sets for *Rankl* (Mm00441908_m1), *Opg* (Mm00435462_m1), *Fgfr1* (Mm00438924_m1), *Fgfr3* (Mm00433294_m1) and the normalizer *Hprt* (Mm00446968_m1) were obtained from Life Technologies. Normalized fold-expression values for *Rankl*, *Opg*, *Fgfr1* and *Fgfr3* were calculated using relative starting quantity values obtained using standard curve qPCR and normalized by relative starting quantity values obtained from standard curve *Hprt* qPCR.

Statistical analysis

All experimental values were analyzed using GraphPad PRISM (v6.0, La Jolla, CA, USA). When experimental conditions involved two groups, an unpaired *t*-test was used to determine differences between groups with significance determined by obtaining a *P*-value of <0.05. When experimental conditions involved three or more groups, one-way ANOVA was used to determine differences between groups. If differences were detected by ANOVA ($P < 0.05$), *post hoc* significance was calculated by Holm-Sidak's method correcting for multiple comparisons with significance determined by obtaining an adjusted *P*-value of <0.05. For analyses tracking body length and weight, repeated measure two-way ANOVA was used; *post hoc* calculated significance, if any, is graphed only for the terminal time point (P18). Graphs of growth plate zone lengths were graphed as grouped analyses for space saving purposes but were analyzed by one-way ANOVA at each time point specified. Data are presented as mean ± SEM.

Supplementary Material

Supplementary Material is available at *HMG* online.

Acknowledgements

We thank Ms Lingzhen Li for technical assistance with *in situ* hybridizations. We thank Dr Douglas Mortlock (Vanderbilt University, Nashville, TN, USA) for the *Fgfr1* and *Fgfr3* ISH probes. We thank Dr Steven Pregizer for providing the *Col10-Cre;LacZ* pups for β-galactosidase staining and for further breeding with the *Nf1* floxed mice. We thank Drs Joey Barnett, Ela Knapik, T. Jack Martin and Jonathan Schoenecker for their critical insight on these studies.

Conflict of Interest statement. None declared.

Funding

This work was supported by the National Institutes of Health (5T32GM007628-37 to Joey Barnett/M.R.K and 5R01AR055966-05

to F.E.); the Children's Tumor Foundation (YIA-2013-01-018 to M.R.K.); and the Department of Defense (W81XWH-09-01-0207 to F.E.).

References

1. Kronenberg, H.M. (2003) Developmental regulation of the growth plate. *Nature*, **423**, 332–336.
2. Lefebvre, V. and Bhattaram, P. (2010) Vertebrate Skeletogenesis. *Curr. Top. Dev. Biol.*, **90**, 291–317.
3. Spranger, J. (2005) Skeletal dysplasias. In: Hall, JG (eds), *Human Malformations and Related Anomalies*. Oxford University Press, USA, pp. 997–1020.
4. Abou-Khalil, R. and Colnot, C. (2014) Cellular and molecular bases of skeletal regeneration: what can we learn from genetic mouse models? *Bone*, **64**, 211–221.
5. Peters, K.G., Werner, S., Chen, G. and Williams, L.T. (1992) Two FGF receptor genes are differentially expressed in epithelial and mesenchymal tissues during limb formation and organogenesis in the mouse. *Development*, **114**, 233–243.
6. Peters, K., Ornitz, D., Werner, S. and Williams, L. (1993) Unique expression pattern of the FGF receptor 3 gene during mouse organogenesis. *Dev. Biol.*, **155**, 423–430.
7. Jacob, A.L., Smith, C., Partanen, J. and Ornitz, D.M. (2006) Fibroblast growth factor receptor 1 signaling in the osteochondrogenic cell lineage regulates sequential steps of osteoblast maturation. *Dev. Biol.*, **296**, 315–328.
8. Delezoide, A.L., Benoist-Lasselin, C., Legeai-Mallet, L., Le Merrer, M., Munnich, A., Vekemans, M. and Bonaventure, J. (1998) Spatio-temporal expression of FGFR 1, 2 and 3 genes during human embryo-fetal ossification. *Mech. Dev.*, **77**, 19–30.
9. Deng, C., Wynshaw-Boris, A., Zhou, F., Kuo, A. and Leder, P. (1996) Fibroblast growth factor receptor 3 is a negative regulator of bone growth. *Cell*, **84**, 911–921.
10. Sahni, M., Raz, R., Coffin, J.D., Levy, D. and Basilico, C. (2001) STAT1 mediates the increased apoptosis and reduced chondrocyte proliferation in mice overexpressing FGF2. *Development*, **128**, 2119–2129.
11. Murakami, S., Balmes, G., McKinney, S., Zhang, Z., Givol, D. and de Crombrugghe, B. (2004) Constitutive activation of MEK1 in chondrocytes causes Stat1-independent achondroplasia-like dwarfism and rescues the Fgfr3-deficient mouse phenotype. *Genes Dev.*, **18**, 290–305.
12. Iwata, T., Chen, L., Li, C., Ovchinnikov, D.A., Behringer, R.R., Francomano, C.A. and Deng, C.X. (2000) A neonatal lethal mutation in FGFR3 uncouples proliferation and differentiation of growth plate chondrocytes in embryos. *Hum. Mol. Gen.*, **9**, 1603–1613.
13. Naski, M.C., Wang, Q., Xu, J. and Ornitz, D.M. (1996) Graded activation of fibroblast growth factor receptor 3 by mutations causing achondroplasia and thanatophoric dysplasia. *Nat. Genet.*, **13**, 233–237.
14. Tavormina, P.L., Shiang, R., Thompson, L.M., Zhu, Y.Z., Wilkin, D.J., Lachman, R.S., Wilcox, W.R., Rimoin, D.L., Cohn, D.H. and Wasmuth, J.J. (1995) Thanatophoric dysplasia (types I and II) caused by distinct mutations in fibroblast growth factor receptor 3. *Nat. Genet.*, **9**, 321–328.
15. Rousseau, F., Bonaventure, J., Legeai-Mallet, L., Pelet, A., Rozet, J.M., Maroteaux, P., Le Merrer, M. and Munnich, A. (1994) Mutations in the gene encoding fibroblast growth factor receptor-3 in achondroplasia. *Nature*, **371**, 252–254.
16. Shiang, R., Thompson, L.M., Zhu, Y.Z., Church, D.M., Fielder, T.J., Bocian, M., Winokur, S.T. and Wasmuth, J.J. (1994) Mutations in the transmembrane domain of FGFR3 cause the most common genetic form of dwarfism, achondroplasia. *Cell*, **78**, 335–342.
17. Wang, Y., Spatz, M.K., Kannan, K., Hayk, H., Avivi, A., Gorivodsky, M., Pines, M., Yayon, A., Lonai, P. and Givol, D. (1999) A mouse model for achondroplasia produced by targeting fibroblast growth factor receptor 3. *Proc. Natl Acad. Sci. USA*, **96**, 4455–4460.
18. Su, W.C., Kitagawa, M., Xue, N., Xie, B., Garofalo, S., Cho, J., Deng, C., Horton, W.A. and Fu, X.Y. (1997) Activation of Stat1 by mutant fibroblast growth-factor receptor in thanatophoric dysplasia type II dwarfism. *Nature*, **386**, 288–292.
19. Li, C., Chen, L., Iwata, T., Kitagawa, M., Fu, X.Y. and Deng, C.X. (1999) A Lys644Glu substitution in fibroblast growth factor receptor 3 (FGFR3) causes dwarfism in mice by activation of STATs and ink4 cell cycle inhibitors. *Hum. Mol. Gen.*, **8**, 35–44.
20. Muenke, M., Schell, U., Hehr, A., Robin, N.H., Losken, H.W., Schinzel, A., Pulleyn, L.J., Rutland, P., Reardon, W. and Malcolm, S. (1994) A common mutation in the fibroblast growth factor receptor 1 gene in Pfeiffer syndrome. *Nat. Genet.*, **8**, 269–274.
21. Schell, U., Hehr, A., Feldman, G.J., Robin, N.H., Zackai, E.H., de Die-Smulders, C., Viskochil, D.H., Stewart, J.M., Wolff, G. and Ohashi, H. (1995) Mutations in FGFR1 and FGFR2 cause familial and sporadic Pfeiffer syndrome. *Hum. Mol. Gen.*, **4**, 323–328.
22. Roscioli, T., Flanagan, S., Kumar, P., Masel, J., Gattas, M., Hyland, V.J. and Glass, I.A. (2000) Clinical findings in a patient with FGFR1 P252R mutation and comparison with the literature. *Am. J. Med. Genet.*, **93**, 22–28.
23. White, K.E., Cabral, J.M., Davis, S.I., Fishburn, T., Evans, W.E., Ichikawa, S., Fields, J., Yu, X., Shaw, N.J., McLellan, N.J. *et al.* (2005) Mutations that cause osteoglophonic dysplasia define novel roles for FGFR1 in bone elongation. *Am. J. Hum. Genet.*, **76**, 361–367.
24. Farrow, E.G., Davis, S.I., Mooney, S.D., Beighton, P., Mascarenhas, L., Gutierrez, Y.R., Pitukcheewanont, P. and White, K.E. (2006) Extended mutational analyses of FGFR1 in osteoglophonic dysplasia. *Am. J. Med. Genet.*, **140A**, 537–539.
25. Sklower Brooks, S., Kassner, G., Qazi, Q., Keogh, M.J. and Gorlin, R.J. (1996) Osteoglophonic dysplasia: review and further delineation of the syndrome. *Am. J. Med. Genet.*, **66**, 154–162.
26. Beighton, P., Cremin, B. and Kozlowski, K. (1980) Osteoglophonic dwarfism. *Pediatr. Radiol.*, **10**, 46–50.
27. Azouz, E.M. and Kozlowski, K. (1997) Osteoglophonic dysplasia: appearance and progression of multiple nonossifying fibromata. *Pediatr. Radiol.*, **27**, 75–78.
28. Kelley, R.I., Borns, P.F., Nichols, D. and Zackai, E.H. (1983) Osteoglophonic dwarfism in two generations. *J. Med. Genet.*, **20**, 436–440.
29. Lemmon, M.A. and Schlessinger, J. (2010) Cell signaling by receptor tyrosine kinases. *Cell*, **141**, 1117–1134.
30. Traverse, S., Gomez, N., Paterson, H., Marshall, C. and Cohen, P. (1992) Sustained activation of the mitogen-activated protein (MAP) kinase cascade may be required for differentiation of PC12 cells. Comparison of the effects of nerve growth factor and epidermal growth factor. *Biochem. J.*, **288**, 351–355.
31. Raucci, A., Laplantine, E., Mansukhani, A. and Basilico, C. (2004) Activation of the ERK1/2 and p38 Mitogen-activated Protein Kinase Pathways Mediates Fibroblast Growth Factor-induced Growth Arrest of Chondrocytes. *J. Biol. Chem.*, **279**, 1747–1756.
32. Crawford, A.H. and Bagamery, N. (1986) Osseous manifestations of neurofibromatosis in childhood. *J. Pediatr. Orthop.*, **6**, 72–88.
33. Crawford, A.H. and Schorry, E.K. (1999) Neurofibromatosis in children: the role of the orthopaedist. *J. Am. Acad. Orthop. Surg.*, **7**, 217–230.

34. Kuorilehto, T., Pöyhönen, M., Bloigu, R., Heikkinen, J., Väänänen, K. and Peltonen, J. (2004) Decreased bone mineral density and content in neurofibromatosis type 1: lowest local values are located in the load-carrying parts of the body. *Osteoporos. Int.*, **16**, 928–936.
35. Stevenson, D.A., Moyer-Mileur, L.J., Murray, M., Slater, H., Sheng, X., Carey, J.C., Dube, B. and Viskochil, D.H. (2007) Bone mineral density in children and adolescents with neurofibromatosis type 1. *J. Pediatr.*, **150**, 83–88.
36. Elefteriou, F., Kolanczyk, M., Schindeler, A., Viskochil, D.H., Hock, J.M., Schorry, E.K., Crawford, A.H., Friedman, J.M., Little, D., Peltonen, J. *et al.* (2009) Skeletal abnormalities in neurofibromatosis type 1: approaches to therapeutic options. *Am. J. Med. Genet.*, **149A**, 2327–2338.
37. Wang, W., Nyman, J.S., Ono, K., Stevenson, D.A., Yang, X. and Elefteriou, F. (2011) Mice lacking Nf1 in osteochondroprogenitor cells display skeletal dysplasia similar to patients with neurofibromatosis type I. *Hum. Mol. Gen.*, **20**, 3910–3924.
38. Ono, K., Karolak, M.R., Ndong, J.deL.C., Ndong, J.D.L.C., Wang, W., Yang, X. and Elefteriou, F. (2013) The ras-GTPase activity of neurofibromin restrains ERK-dependent FGFR signaling during endochondral bone formation. *Hum. Mol. Gen.*, **22**, 3048–3062.
39. Zhou, Y.X., Xu, X., Chen, L., Li, C., Brodie, S.G. and Deng, C.X. (2000) A Pro250Arg substitution in mouse Fgfr1 causes increased expression of Cbfa1 and premature fusion of calvarial sutures. *Hum. Mol. Gen.*, **9**, 2001–2008.
40. Kuorilehto, T., Nissinen, M., Koivunen, J., Benson, M.D. and Peltonen, J. (2004) NF1 tumor suppressor protein and mRNA in skeletal tissues of developing and adult normal mouse and NF1-deficient embryos. *J. Bone Miner. Res.*, **19**, 983–989.
41. Ndong, J.D.L.C., Makowski, A.J., Uppuganti, S., Vignaux, G., Ono, K., Perrien, D.S., Joubert, S., Baglio, S.R., Granchi, D., Stevenson, D.A. *et al.* (2014) Asfotase-α improves bone growth, mineralization and strength in mouse models of neurofibromatosis type-1. *Nat. Med.*, **20**, 904–910.
42. Gebhard, S., Hattori, T., Bauer, E., Schlund, B., Bösl, M.R., de Crombrugghe, B. and Mark,, von der, K. (2008) Specific expression of Cre recombinase in hypertrophic cartilage under the control of a BAC-Col10a1 promoter. *Matrix Biol.*, **27**, 693–699.
43. Soriano, P. (1999) Generalized lacZ expression with the ROSA26 Cre reporter strain. *Nat. Genet.*, **21**, 70–71.
44. Golovchenko, S., Hattori, T., Hartmann, C., Gebhardt, M., Gebhard, S., Hess, A., Pausch, F., Schlund, B. and Mark,, von der, K. (2013) Deletion of beta catenin in hypertrophic growth plate chondrocytes impairs trabecular bone formation. *Bone*, **55**, 102–112.
45. Xiong, J., Onal, M., Jilka, R.L., Weinstein, R.S., Manolagas, S.C. and O'Brien, C.A. (2011) Matrix-embedded cells control osteoclast formation. *Nat. Med.*, **17**, 1235–1241.
46. Wang, Q., Green, R.P., Zhao, G. and Ornitz, D.M. (2001) Differential regulation of endochondral bone growth and joint development by FGFR1 and FGFR3 tyrosine kinase domains. *Development*, **128**, 3867–3876.
47. Guagnano, V., Furet, P., Spanka, C., Bordas, V., Le Douget, M., Stamm, C., Brueggen, J., Jensen, M.R., Schnell, C., Schmid, H. *et al.* (2011) Discovery of 3-(2,6-Dichloro-3,5-dimethoxy-phenyl)-1-{6-[4-(4-ethyl-piperazin-1-yl)-phenylamino]-pyrimidin-4-yl}-1-methyl-urea (NVP-BGJ398), A Potent and Selective Inhibitor of the Fibroblast Growth Factor Receptor Family of Receptor Tyrosine Kinase. *J. Med. Chem.*, **54**, 7066–7083.
48. Sahni, M., Ambrosetti, D.C., Mansukhani, A., Gertner, R., Levy, D. and Basilico, C. (1999) FGF signaling inhibits chondrocyte proliferation and regulates bone development through the STAT-1 pathway. *Genes Dev.*, **13**, 1361–1366.
49. Eswarakumar, V.P., Lax, I. and Schlessinger, J. (2005) Cellular signaling by fibroblast growth factor receptors. *Cytokine Growth Factor Rev.*, **16**, 139–149.
50. Lax, I., Wong, A., Lamothe, B., Lee, A., Frost, A., Hawes, J. and Schlessinger, J. (2002) The docking protein FRS2alpha controls a MAP kinase-mediated negative feedback mechanism for signaling by FGF receptors. *Mol. Cell*, **10**, 709–719.
51. Naski, M.C., Colvin, J.S., Coffin, J.D. and Ornitz, D.M. (1998) Repression of hedgehog signaling and BMP4 expression in growth plate cartilage by fibroblast growth factor receptor 3. *Development*, **125**, 4977–4988.
52. Colvin, J.S., Bohne, B.A., Harding, G.W., McEwen, D.G. and Ornitz, D.M. (1996) Skeletal overgrowth and deafness in mice lacking fibroblast growth factor receptor 3. *Nat. Genet.*, **12**, 390–397.
53. Elefteriou, F., Benson, M.D., Sowa, H., Starbuck, M., Liu, X., Ron, D., Parada, L.F. and Karsenty, G. (2006) ATF4 mediation of NF1 functions in osteoblast reveals a nutritional basis for congenital skeletal dysplasiae. *Cell Metab.*, **4**, 441–451.
54. Provot, S., Nachtrab, G., Paruch, J., Chen, A.P., Silva, A. and Kronenberg, H.M. (2008) A-raf and B-raf are dispensable for normal endochondral bone development, and parathyroid hormone-related peptide suppresses extracellular signal-regulated kinase activation in hypertrophic chondrocytes. *Mol. Cell. Biol.*, **28**, 344–357.
55. Sebastian, A., Matsushita, T., Kawanami, A., Mackem, S., Landreth, G.E. and Murakami, S. (2011) Genetic inactivation of ERK1 and ERK2 in chondrocytes promotes bone growth and enlarges the spinal canal. *J. Orthop. Res.*, **29**, 375–379.
56. Yang, X., Harkins, L.K., Zubanova, O., Harrington, A., Kovalenko, D., Nadeau, R.J., Chen, P.-Y., Toher, J.L., Lindner, V., Liaw, L. *et al.* (2008) Overexpression of Spry1 in chondrocytes causes attenuated FGFR ubiquitination and sustained ERK activation resulting in chondrodysplasia. *Dev. Biol.*, **321**, 64–76.
57. Legeai-Mallet, L., Benoist-Lasselin, C., Delezoide, A.L., Munnich, A. and Bonaventure, J. (1998) Fibroblast growth factor receptor 3 mutations promote apoptosis but do not alter chondrocyte proliferation in thanatophoric dysplasia. *J. Biol. Chem.*, **273**, 13007–13014.
58. Stevenson, D.A., Little, D., Armstrong, L., Crawford, A.H., Eastwood, D., Friedman, J.M., Greggi, T., Gutierrez, G., Hunter-Schaedle, K., Kendler, D.L. *et al.* (2013) Approaches to treating NF1 tibial pseudarthrosis: consensus from the children's tumor foundation NF1 bone abnormalities consortium. *J. Pediatr. Orthop.*, **33**, 269–275.
59. Ovchinnikov, D.A., Deng, J.M., Ogunrinu, G. and Behringer, R.R. (2000) Col2a1-directed expression of Cre recombinase in differentiating chondrocytes in transgenic mice. *Genesis*, **26**, 145–146.
60. Zhu, Y., Romero, M.I., Ghosh, P., Ye, Z., Charnay, P., Rushing, E. J., Marth, J.D. and Parada, L.F. (2001) Ablation of NF1 function in neurons induces abnormal development of cerebral cortex and reactive gliosis in the brain. *Genes Dev.*, **15**, 859–876.
61. Hoch, R.V. and Soriano, P. (2006) Context-specific requirements for Fgfr1 signaling through Frs2 and Frs3 during mouse development. *Development*, **133**, 663–673.
62. Takeda, S., Bonnamy, J.P., Owen, M.J., Ducy, P. and Karsenty, G. (2001) Continuous expression of Cbfa1 in nonhypertrophic chondrocytes uncovers its ability to induce hypertrophic chondrocyte differentiation and partially rescues Cbfa1-deficient mice. *Genes Dev.*, **15**, 467–481.
63. Ducy, P., Zhang, R., Geoffroy, V., Ridall, A.L. and Karsenty, G. (1997) Osf2/Cbfa1: a transcriptional activator of osteoblast differentiation. *Cell*, **89**, 747–754.